Green Sciences
Volume 28 Issue 1 · pp. 17–32 · DOI: 10.2478/pjct-2026-0002

Numerical study on the influence of outlet diameters on the discharge characteristics of dual-outlet silos

Research Article

Xuanyi Liu[1,2]*, Fei Wang[1,2], Sijiu Qi[1,2]

[1] China Energy Science and Technology Research Institute Co., Ltd., Nanjing, 210046, China
[2] State Key Laboratory of Low-Carbon Smart Coal-Fired Power Generation and Ultra-Clean Emission, Nanjing, 210023, China

Received 30 September 2025; Accepted 08 February 2026

Abstract: The efficient and safe discharge of powders from multi-outlet silos is critical in many industrial processes. This study applied a two-fluid model to investigate powder-gas dynamics in a dual-outlet silo with outlet diameters of 0.26–0.78 m. Results show that larger outlets accelerate subsidence of the free surface, deepen local depressions, and significantly raise particle velocities, leading to expansion of rapid-flow regions near the outlets. The powder volume fraction exhibits a W-shaped profile in the upper silo and a V-shaped distribution close to the outlets, reflecting the combined effects of gravity and silo geometry. Negative pressure zones consistently emerge above the outlets during early discharge; increasing outlet size not only amplifies these pressure peaks but also promotes faster recovery. Moreover, slight competitive effects between the two outlets were identified, indicating interaction in discharge pathways. These findings demonstrate that outlet diameter is a critical parameter governing both flow dynamics and discharge performance in dual-outlet silos.

Keywords: *Numerical simulation • Two-fluid model • Dual-outlet silo • Outlet diameter • Discharge characteristics.*

1. Introduction

With the large-scale integration of renewable energy into power systems, coal-fired power plants worldwide are increasingly transitioning from base-load providers to flexible regulating units [1]. Consequently, long-term operation under low-load conditions and frequent start–stop cycles has become the new normal. This shift places much higher demands on coal-fired units, particularly on the pulverized coal feeding system, which must deliver a stable and responsive fuel supply across a wide range of fluctuating operating conditions. Under deep peak-shaving scenarios, however, the feeding system often struggles to meet these requirements. Problems such as coal flow fluctuations, transport obstructions, and maldistribution are frequently encountered, especially at low load. These instabilities not only disturb the furnace combustion process but also degrade the load-following capability of the unit and overall operational stability. In severe cases, they may even trigger hazardous events such as primary air duct blockages or boiler flameouts, thereby threatening both the safety and economic performance of the plant.

As a critical component of the coal feeding system, the multi-outlet pulverized coal silo plays a decisive role in ensuring the continuity and stability of fuel supply. Among the factors governing bulk material flow, the outlet size is one of the most influential parameters. It determines the ease of flow initiation, the uniformity of discharge across outlets, and the overall stability of silo performance [2]. A comprehensive understanding of the effect of outlet size on discharge characteristics in multi-outlet silos is therefore essential for optimizing silo design and improving the reliability of coal feeding systems under flexible operation of coal-fired units.

Systematic investigations into the discharge characteristics of powder silos can be traced back to the pioneering work of Jenike in the 1960s [3,4]. Jenike proposed the well-known shear test method, formulated the fundamental theory of powder flowability, and developed silo design charts [4]. Around the same period, Beverloo et al. [5]

* *E-mail: 12011340@ceic.com*

Open Access. © 2026 Xuanyi Liu *et al.*, published by West Pomeranian University of Technology, Szczecin
This work is licensed under the Creative Commons Attribution-NonCommercial-NoDerivs 4.0 License.

introduced the classical Beverloo equation, which has since become a benchmark model for predicting the mass flow rate of granular discharge through a single outlet.

Over the past decades, research attention has gradually shifted from static design considerations toward the dynamic evolution of stress fields within silos during discharge [6–8], as well as the effects of structural modifications – such as inserts on flow regimes [9–11] and curved hoppers on discharge characteristics [12–15]. Wang et al. [16] reported oscillatory behavior of normal wall stresses in mass-flow silos, attributing this phenomenon to macro-slip of the granular solid against the silo wall. By using spherical glass beads as model materials, Wang et al. [17] observed periodic fluctuations in wall stresses, particularly at the transition zone between the cylindrical and conical sections, highlighting the sensitivity of stress states to local geometry. Wójcik et al. [18] investigated various insert geometries (e.g., double-cone, cone-in-cone, inverted-cone) with respect to their influence on flow patterns and wall stress distributions, and provided guidelines for their selection and placement to achieve optimal flow conditions. Huang et al. [19] experimentally investigated the effect of curved hoppers on mass discharge rates, showing that hoppers optimized using their method achieved discharge rates over 100% higher than conventional conical hoppers.

With the rapid development of numerical techniques, simulations have become essential approaches in silo discharge studies, with methods such as the discrete element method [20–22], the finite element method [8,23], and the two-fluid model (TFM) [24,25] being extensively applied to capture the complex interactions between granular assemblies and confining boundaries. For fine powders, where interstitial fluid effects cannot be neglected [26], the TFM – treating both solid and fluid phases as interpenetrating continua – has exhibited distinct advantages. For instance, Audard et al. [27] employed a two-fluid Euler–Euler model to simulate powder discharge from a silo, successfully reproducing mass flow rates and analyzing the mechanisms behind granular jet expansion.

However, the discharge behavior of multi-outlet silos has received comparatively limited attention despite its practical importance in industrial applications [28]. Xu et al. [28] conducted quasi-two-dimensional silo experiments and showed that outlet spacing governed flow coupling, with closely spaced outlets enhancing overall discharge rates. Dai et al. [29] experimentally investigated the discharge of cohesive particles from a two-outlet silo and found that the discharge rate with two outlets was approximately 1.1–1.6 times that with a single outlet. Lee et al. [30] developed and validated a kinematic theory-based model to predict the profiles of the top and mixed loading surfaces during discharge from multiple-outlet silos, aiding volume estimation and efficient operation. From the literature reviewed, studies on the influence of outlet size on the discharge dynamics of dual-outlet silos remain limited. Given the decisive role of outlet size in governing discharge behavior, further research is clearly needed to advance mechanistic understanding and support the effective design of multi-outlet silo systems.

In the present study, a TFM was employed to numerically investigate the coupled dynamics of powders and interstitial gas in a dual-outlet silo system. Three outlet diameters, ranging from 0.26 to 0.78 m, were considered to examine their influence on the discharge process. The spatial and temporal distributions of powder volume fraction, gas pressure, and particle velocity, as well as the overall discharge characteristics, were analyzed in detail. The results contribute to a better understanding of the role of outlet size in governing the coupled flow behavior and offer guidance for the optimized design of multi-outlet silo systems.

2. Model description

2.1 Physical model

In industrial applications, multi-outlet silos are commonly designed by combining an integrated upper storage bin with a lower multirow dual-outlet hopper [29]. To simplify modeling and computation, a two-dimensional dual-outlet model, as illustrated in Figure 1, was introduced in this study to simulate the discharge behavior. The use of a two-dimensional configuration in this study was a deliberate simplification to enable detailed analysis of the underlying flow mechanisms at a manageable computational cost. The main assumptions are as follows: (1) the silo is sufficiently wide such that wall effects in the out-of-plane direction are minimal; (2) the main flow structures (such as funnel flow and mass flow) are dominated by gravity and outlet geometry, which can be qualitatively captured in 2D; and (3) the flow is symmetric with respect to the silo mid-plane. The corresponding geometric parameters are listed in Table 1. The model consisted of a silo and its associated vertical pipes. The silo height L_1 was 7.05 m, while the pipe length L_2 was 3.00 m. The silo wall was inclined at 15° relative to the vertical. In the lower part of the silo, an inverted V-shaped structure was located at the center to split the powder flow into two outlets, with a base

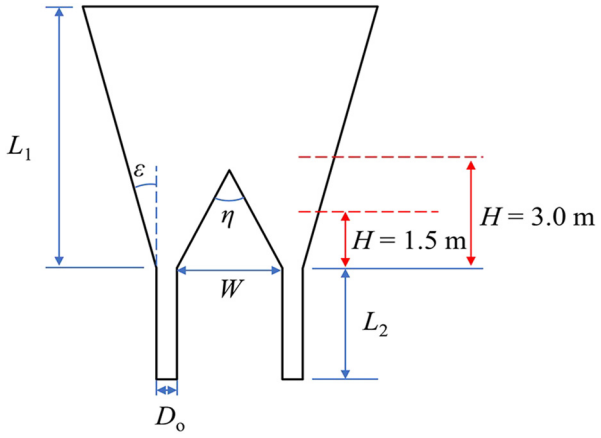


Figure 1. Schematic diagram of the dual-outlet silo.

Source: Author's contribution.

Table 1. Model geometry and parameter values

Parameter	Value
L_1 (m)	7.05
L_2 (m)	3.00
W (m)	2.23
D_o (m)	0.26, 0.52, 0.78
ε (°)	15.0
η (°)	54.0
d_p (μm)	200
ϕ_e (°)	30

Source: Author's contribution.

width W of 2.23 m and an apex angle of 54°. Both hopper outlets had the same diameter. In this study, three different outlet diameters were investigated, namely, D_o = 0.26, 0.52, and 0.78 m. In the current 2D model, the outlet diameter was increased by shifting the two side walls laterally outward, and the bin width at the top location varied accordingly.

The gas phase was modeled as air at ambient conditions, with a density of 1.225 kg/m^3 and a viscosity of 1.8×10^{-5} Pa s. The solid phase represents dry coal powder, with a particle density of 1,400 kg/m^3. The powder particles had a diameter of 200 μm, and the initial fill height was 9.00 m above the pipe outlet. The particle density, ρ_p, was measured by an automatic true-density analyzer (Micromeritics, AccuPyc-1330). The effective angle of internal friction, ϕ_e, was 30° tested by a direct shear tester (Geocomp ShearTrac II, USA). The specific physical parameters of the powder materials are shown in Table 1.

2.2 Numerical model

In this study, the discharge process of powder within the silo and vertical pipes was simulated using a TFM. The TFM is a mathematical framework used to simulate and analyze the interactions between different phases in multiphase flow systems, and it has been widely applied in studies of gas–liquid, liquid–solid, and gas–solid two-phase flows [31]. In this model, each phase is treated as a separate continuous medium, and the coupling and interactions between the phases, such as momentum transfer, mass exchange, and energy transfer, are represented in the form of source terms. Accordingly, the mathematical model employed in this study is described from three aspects: the gas phase model, the solid phase model, and the gas–solid interaction model.

2.2.1 Gas phase model

The gas phase model consisted of governing equations and constitutive equations. The governing equations for the gas phase include the continuity equation and the momentum equation, which are presented as equations (1) and (2), respectively.

$$\frac{\partial}{\partial t}(\alpha_g \rho_g) + \nabla \cdot (\alpha_g \rho_g \mathbf{v}_g) = 0 \tag{1}$$

where α_g is the gas volume fraction, $\boldsymbol{v}_g$ is the gas velocity vector, and ρ_g is the gas density.

$$\frac{\partial}{\partial t}(\alpha_g \rho_g \mathbf{v}_g) + \nabla \cdot (\alpha_g \rho_g \mathbf{v}_g \mathbf{v}_g) = -\alpha_g \nabla P_g + \nabla \cdot \bar{\bar{\tau}}_g - \beta(\mathbf{v}_g - \mathbf{v}_s) + \alpha_g \rho_g \mathbf{g} \tag{2}$$

where P_g is the gas pressure, $\overline{\overline{\tau}}_g$ is the gas phase stress tensor, β is the interphase momentum exchange coefficient, $\boldsymbol{v}_s$ is the solid velocity vector, and g is the gravitational acceleration. On the right-hand side of the equation, the terms represent the pressure gradient, the divergence of the viscous stress, the interphase interaction force (e.g., drag), and the gravitational source term.

Considering that the silo discharge process exhibited typical characteristics of slow dense flow, the gas phase was modeled as an incompressible Newtonian fluid, with turbulence effects being neglected. Accordingly, the constitutive equation for the gas phase stress tensor can be expressed as follows:

$$\overline{\overline{\tau}}_g = 2\alpha_g\mu_g\overline{\overline{D}}_g - \frac{2}{3}\alpha_g\mu_g tr(\overline{\overline{D}}_g)\overline{\overline{I}} \tag{3}$$

where μ_g denotes the gas dynamic viscosity and $\overline{\overline{D}}_g$ is the gas-phase rate of strain tensor, which can be calculated by

$$\overline{\overline{D}}_g = \frac{1}{2}[(\nabla\mathbf{v}_g) + (\nabla\mathbf{v}_g)^T] \tag{4}$$

2.2.2 Solid phase model

The governing equations for the solid phase (i.e., the particulate phase) included the continuity equation, the momentum equation, and the granular temperature transport equation [32], which are expressed as equations (5)–(7), respectively.

$$\frac{\partial}{\partial t}(\alpha_s\rho_s) + \nabla\cdot(\alpha_s\rho_s\mathbf{v}_s) = 0 \tag{5}$$

where α_s is the solid volume fraction and ρ_s is the solid density.

$$\frac{\partial}{\partial t}(\alpha_s\rho_s\mathbf{v}_s) + \nabla\cdot(\alpha_s\rho_s\mathbf{v}_s\mathbf{v}_s) = -\alpha_s\nabla P_g - \nabla P_s + \nabla\cdot\overline{\overline{\tau}}_s + \beta(\mathbf{v}_g - \mathbf{v}_s) + \alpha_s\rho_s\mathbf{g} \tag{6}$$

where P_s is the solid pressure and $\overline{\overline{\tau}}_s$ is the solid stress tensor.

$$\frac{3}{2}\left[\frac{\partial}{\partial t}(\alpha_s\rho_s\Theta) + \nabla\cdot(\alpha_s\rho_s\boldsymbol{v}_s\Theta)\right] = (-P_{s,kc}\overline{\overline{I}} + \overline{\overline{\tau}}_{s,kc}) : \nabla\boldsymbol{v}_s - \nabla\cdot(\kappa_s\nabla\Theta) - J_{coll} - J_{vis} \tag{7}$$

On the right-hand side of equation (7), the four terms correspond respectively to the granular kinetic energy fluctuations induced by shear deformation, the spatial transport of granular temperature due to diffusion, the dissipation of kinetic energy due to inelastic collisions, and the viscous dissipation arising from interparticle friction and particle-fluid interactions. In this equation, Θ denotes the granular temperature, which characterizes the intensity of particle velocity fluctuations, $P_{s,kc}$ represents the kinetic-collisional pressure, $\overline{\overline{\tau}}_{s,kc}$ denotes the kinetic-collisional stress tensor, and κ_s represents the diffusion coefficient. The corresponding expressions for these terms are given as follows:

$$\Theta = \frac{1}{3}\overline{\boldsymbol{v}_s^2} \tag{8}$$

$$P_{s,kc} = \alpha_s\rho_s\Theta + 2\rho_s(1+e)\alpha_s^2 g_0\Theta \tag{9}$$

$$\overline{\overline{\tau}}_{s,kc} = 2\alpha_s\mu_{s,kc}\overline{\overline{D}}_s + \alpha_s\left(\lambda_{s,kc} - \frac{2}{3}\mu_{s,kc}\right)tr(\overline{\overline{D}}_s)\overline{\overline{I}} \tag{10}$$

$$\kappa_s = \frac{15 d_s\rho_s\alpha_s\sqrt{\Theta\pi}}{4(41-33\eta)}\left[1 + \frac{12}{5}\eta^2(4\eta-3)\alpha_s g_0 + \frac{16}{15\pi}(41-33\eta)\eta\alpha_s g_0\right] \tag{11}$$

where

$$\eta = \frac{1}{2}(1+e) \tag{12}$$

In equation (9), e is the restitution coefficient and g_0 is the radial distribution function, which accounts for the increased probability of collisions between particles when the solid phase becomes dense. It is calculated as follows:

$$g_0 = \left[1 - \left(\frac{\alpha_s}{\alpha_{s,\max}}\right)^{1/3}\right]^{-1} \tag{13}$$

where $\alpha_{s,max}$ represents the solid volume fraction at the maximum packing limit.

In equation (10), $\mu_{s,kc}$ denotes the shear viscosity of the solid phase, which consists of the kinetic and collisional contributions; $\lambda_{s,kc}$ represents the bulk viscosity of the solid phase, characterizing the resistance of particles to compression and expansion; and $\overline{\overline{D}}_s$ is the solid-phase rate of strain tensor. The detailed expressions of $\mu_{s,kc}$, $\lambda_{s,kc}$, and $\overline{\overline{D}}_s$ are given in equations (14) and (16), respectively.

$$\mu_{s,kc} = \mu_{s,k} + \mu_{s,c} \tag{14}$$

$$\lambda_{s,kc} = \frac{4}{3}\alpha_s^2\rho_s d_s g_0(1+e)\sqrt{\frac{\Theta}{\pi}} \tag{15}$$

$$\overline{\overline{D}}_s = \frac{1}{2}[(\nabla\mathbf{v}_s) + (\nabla\mathbf{v}_s)^T] \tag{16}$$

In equation (14), $\mu_{s,k}$ and $\mu_{s,c}$ can be calculated from the following expressions:

$$\mu_{s,k} = \frac{10\rho_s d_s\sqrt{\Theta\pi}}{96\alpha_s(1+e)g_0}\left[1+\frac{4}{5}g_0\alpha_s(1+e)\right]^2 \tag{17}$$

$$\mu_{s,c} = \frac{4}{5}\alpha_s\rho_s d_s g_0(1+e)\sqrt{\frac{\Theta}{\pi}} \tag{18}$$

In addition, particles in the silo remain in long-term contact and form a stable contact network under quasi-static or slow flow conditions, so that the bulk powder in the silo exhibits mechanical properties similar to those of a continuous solid. Therefore, the description of the solid-phase stress must account for the influence of interparticle friction. Accordingly, in this study, the solid-phase stress tensor $\bar{\bar{\tau}}_s$ and the solid pressure P_s were formulated as the superposition of kinetic and frictional contributions, as given by the following equations [33]:

$$\bar{\bar{\tau}}_s = \bar{\bar{\tau}}_{s,kc} + \bar{\bar{\tau}}_{s,f} \tag{19}$$

$$P_s = P_{s,kc} + P_{s,f} \tag{20}$$

In equation (19), the frictional shear stress tensor $\bar{\bar{\tau}}_{s,f}$ is calculated using the following model [34,35]:

$$\bar{\bar{\tau}}_{s,f} = 2\alpha_s\mu_{s,f}\bar{\bar{D}}_s - \frac{2}{3}\alpha_s\mu_{s,f}tr(\bar{\bar{D}}_s)\bar{\bar{I}} \tag{21}$$

where $\mu_{s,f}$ denotes the frictional viscosity, which can be calculated from the following expression [35]:

$$\mu_{s,f} = \frac{\sqrt{2}P_{s,f}\sin\phi_e}{2\sqrt{\bar{\bar{D}}_s:\bar{\bar{D}}_s+\Theta/d_s^2}} \tag{22}$$

In equation (20), $P_{s,f}$ denotes the frictional pressure, defined as the normal component of the frictional stress, and is calculated as follows:

$$P_{s,f} = \begin{cases} 0 & \alpha_s < \alpha_{s,\min} \\ \mathrm{Fr}\dfrac{(\alpha_s-\alpha_{s,\min})^n}{(\alpha_{s,\max}-\alpha_s)^p} & \alpha_s \geq \alpha_{s,\min} \end{cases} \tag{23}$$

where Fr, n, and p are empirical coefficients related to material properties; $\alpha_{s,min}$ denotes the minimum solid volume fraction at which frictional effects become significant.

2.2.3 Gas–solid interaction model

In this study, momentum exchange between particles and gas is primarily represented by the drag force. The drag force not only significantly influences the evolution of particle velocity but also acts as a coupling term in the momentum equations of both the solid and gas phases. The Gidaspow drag model [36] was adopted here to provide a unified description of drag in both dilute and dense regions. The Gidaspow model combines the features of the Wen and Yu's model [37], suitable for dilute particle regions, and the Ergun's model [38], applicable to dense particle regions. It employs a piecewise formulation based on the solid-phase volume fraction, as detailed below.

$$\beta = \begin{cases} \dfrac{3}{4}C_D\dfrac{\alpha_s\alpha_g\rho_g|\boldsymbol{v}_s-\boldsymbol{v}_g|}{d_s}\alpha_g^{-2.65} & \alpha_s \leq 0.2 \\ 150\dfrac{\alpha_s^2\mu_g}{(1-\alpha_s)d_s^2}+1.75\dfrac{\rho_g\alpha_s|\boldsymbol{v}_s-\boldsymbol{v}_g|}{d_s} & \alpha_s > 0.2 \end{cases} \tag{24}$$

$$C_D = \frac{24}{\alpha_g\,\mathrm{Re}_p}[1+0.15(\alpha_g\,\mathrm{Re}_p)^{0.687}] \tag{25}$$

$$\mathrm{Re}_p = \frac{d_s\rho_g|\boldsymbol{v}_g-\boldsymbol{v}_s|}{\mu_g} \tag{26}$$

2.3 Boundary conditions and solution methods

During the simulation, a no-slip boundary condition was applied to the gas phase at the silo walls, while a partial-slip boundary condition was imposed on the solid phase to better approximate actual operating conditions, as shown in Figure 2. Pressure outlet boundaries were used at both the top of the silo and the bottom of the pipes. The simulation was solved using the phase-coupled SIMPLE algorithm [39,40], with the momentum and volume fraction equations discretized using the QUICK scheme. To ensure numerical stability, the time step was set to 0.0001 s.

3. Results and discussion

3.1 Effect on the powder volume fraction distribution

The variation in the outlet diameter directly affects its flow characteristics, packing state, and discharge stability in the silo. Figure 3(a–c) illustrates the evolution of the powder volume fraction during the discharge process of a dual-outlet silo, with outlet diameters of 0.26 m, 0.52 m, and 0.78 m, respectively. As shown in Figure 3, once the

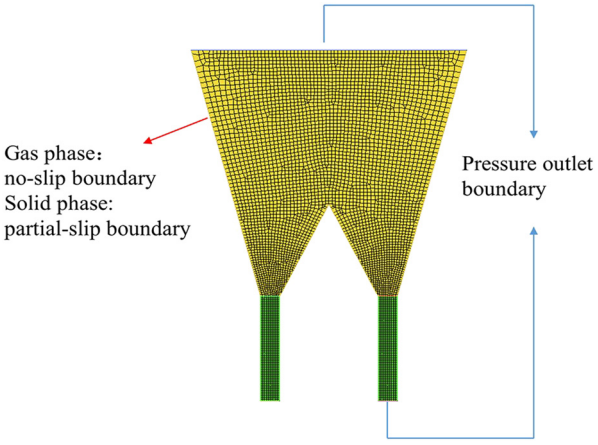


Figure 2. Computational mesh and boundary conditions.

Source: Author's contribution.

silo outlet was opened, a distinct shear band appeared above the outlet, initiating powder flow. In the region above the outlet, particles were accelerated under gravity, which reduced the particle concentration within a unit volume and consequently lowered the local solid volume fraction. Subsequently, the free surface at the top of the powder began to subside, forming a local depression. Meanwhile, the material near the silo walls also flowed downward, and no dead zone was observed. When the free surface subsided near the apex of the inverted V-shaped structure, two local depressions developed above the two outlets. The lowest points of these depressions did not align with the axes of the vertical pipes but deviated inward. This inward deviation was attributed to the asymmetry of the hoppers, i.e., the unequal inclination angles of the hopper walls on both sides affected the shape of the free surface.

The time required for the top free surface of the powder to reach the apex of the inverted V-shaped structure varies with outlet size. For outlet diameters of 0.26, 0.52, and 0.78 m, the corresponding times were 17.0, 8.5, and 6.0 s, respectively. This variation is directly related to the discharge rate, which will be discussed in detail later. Moreover, a larger outlet results in a deeper depression of the free surface when it reaches the apex of the inverted V-shaped structure.

Figure 4 quantitatively compares the lateral solid volume fraction distributions of powders with different outlet diameters at two vertical positions (H = 3 m and H = 1.5 m, as indicated in Figure 1). Owing to the structural characteristics of the silo, where discharge occurred on both sides of the central protrusion, the overall distribution exhibited an approximate W-shaped profile at H = 3.0 m, as shown in Figure 4(a). The range of variation among all cases (0.488–0.494) indicates only a small difference of about 1.4%. In this region, particles were mainly influenced by gravitational settling with weak wall confinement, leading to a slightly denser packing compared with the lower section. At H = 1.5 m, the powder flow was more constrained by the side walls, resulting in a relatively looser packing state. Moreover, the difference in solid volume fraction between the central and near-wall regions became more pronounced. The volume fraction distributions within the two hoppers each displayed a distinct V-shaped pattern, as shown in Figure 4(b).

3.2 Effect on the gas pressure distribution

Figure 5(a–c) illustrates the evolution of gas pressure distributions during the discharge process, allowing a comparative analysis of the effect of the outlet size on gas pressure. As shown in Figure 5, a pronounced negative pressure region existed inside the silo during discharge. Once the outlet was opened, a negative pressure region immediately formed above it and gradually moved downward, eventually stabilizing at the junction between the hopper and the pipe. This phenomenon was primarily caused by the downward movement of solid particles at the onset of discharge, during which the vacated space was not sufficiently filled by air, resulting in negative pressure above the outlet. During subsequent discharge, particle motion near the hopper-pipe junction was relatively intense, and falling particles carried surrounding air downward. Since this region was far from the lower pipe outlet, the replenishment of air was limited, causing the negative pressure region to stabilize at the hopper-pipe junction.

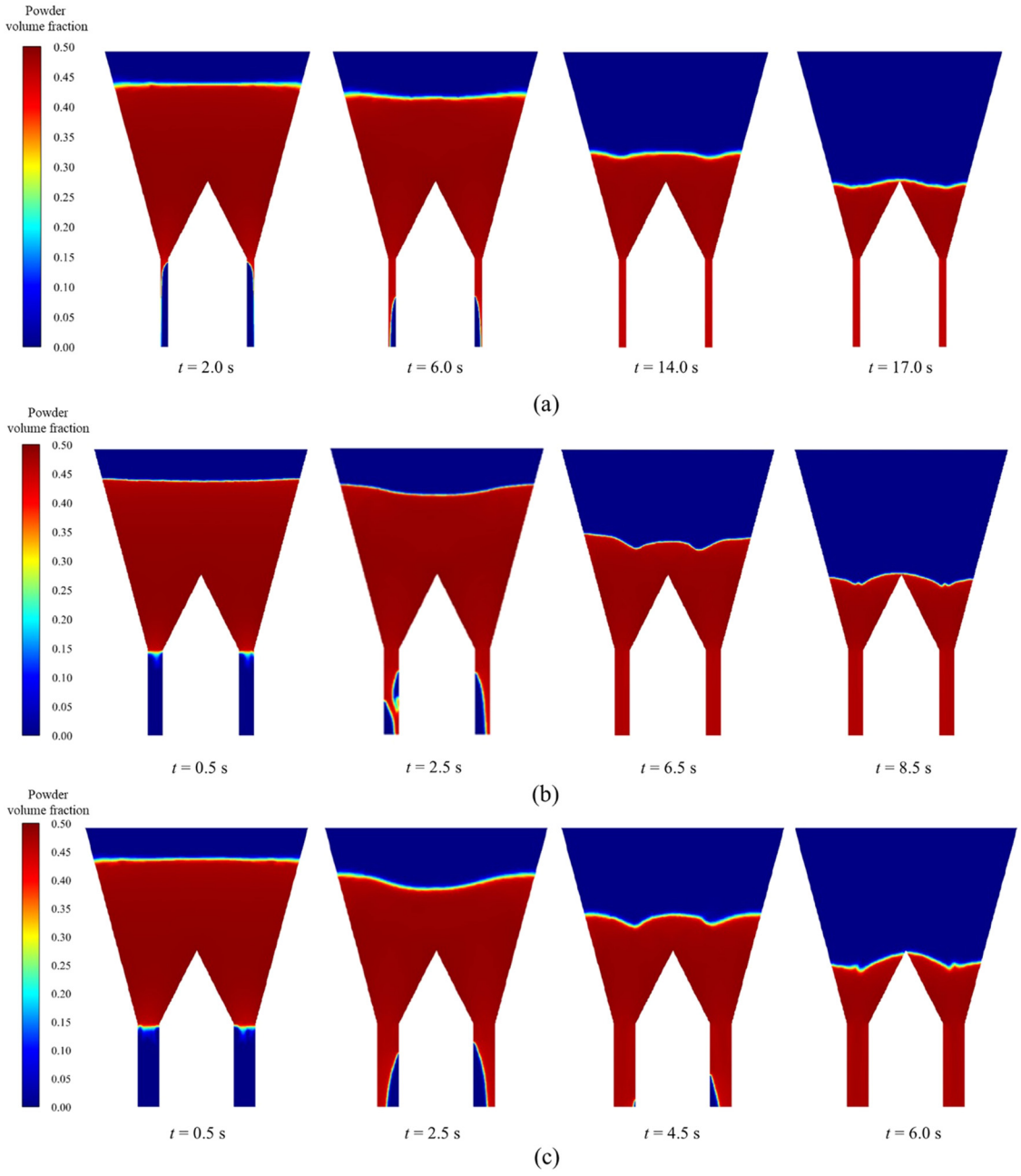


Figure 3. Contours of powder volume fraction in the silo system during discharge. (a) D_o = 0.26 m, (b) D_o = 0.52 m, (c) D_o = 0.78 m.

Source: Author's contribution.

Moreover, at the onset of discharge, the magnitude of the local negative pressure peak increased with the increasing outlet diameter. A larger outlet allowed particles to exit more rapidly, creating voids above the outlet faster than air can refill them. As a result, the local negative pressure became more pronounced for larger outlet diameters. Furthermore, as observed in Figure 5(c), the gas pressure distributions in the two conical hoppers were not entirely identical, which was attributed to the competitive discharge behavior inherent in a dual-outlet silo during the discharge process [41].

Figure 6 presents the temporal evolution of the average gas pressure within the powder during discharge. The average gas pressure shown in the figure was

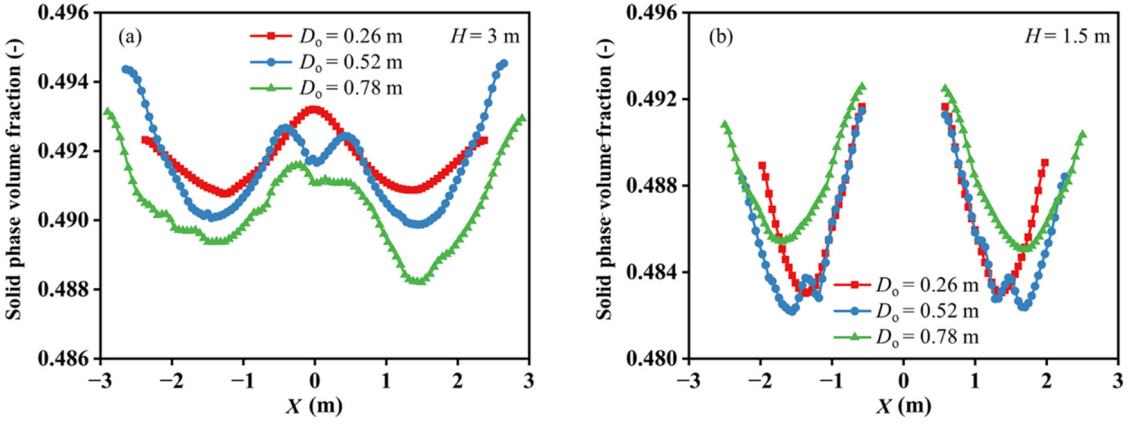


Figure 4. Powder volume fraction at discharge time t = 2.5 s. (a) H = 3.0 m, (b) H = 1.5 m.

Source: Author's contribution.

obtained by performing a spatial integral over the entire computational domain, excluding the outlet pipes. Each data point on the curve represents an instantaneous spatial average. The time step for each instantaneous average was 0.0001 s, and the time interval between adjacent sampling points on the curve was 0.1 s. The average gas pressure curves corresponding to different outlet diameters exhibit three inflection points, dividing the pressure evolution into four distinct stages. During the discharge process, the negative pressure inside the silo underwent a sequence of "increase-decrease-increase-decrease." At the initial stage of discharge, the average gas pressure under different outlet diameters exhibited noticeable fluctuations, reflecting the complex interactions between particles and gas. In the middle and later stages of discharge, the average gas pressure generally showed a relatively stable and nearly linear variation. Before the first inflection point, as the outlet diameter increased, the rate of negative pressure growth (i.e., the slope of the curve) also increased. Before the second inflection point, the rate of negative pressure reduction became larger. After the third inflection point, namely, in the later stage, a larger outlet led to a faster recovery of the pressure. This faster recovery was due to the larger outlet, which allowed air to enter the silo more quickly and subsequently refilled the voids near the hopper-pipe junction more efficiently through the interstitial spaces between particles, resulting in a quicker restoration of gas pressure.

3.3 Effect on the powder velocity distribution

Figure 7 illustrates the evolution of particle velocity distributions within the dual-outlet silo under different outlet diameters. Overall, the evolution trends of the velocity fields were highly consistent across powders with varying outlet diameters. At the initial stage of discharge, particle velocities in the silo region were relatively uniform, whereas the velocity distribution in the pipe region exhibited fluctuations. As the discharge progresses, particularly in the later stages, the powder level in the silo decreased and the particle motion became increasingly influenced by the gas flow. Some particles near the free surface were lifted by the airflow. Meanwhile, particle flow in the pipe gradually stabilized, and the velocity distribution became more uniform. Furthermore, during discharge, a larger outlet diameter resulted in an expanded rapid-flow region. This occurred because a wider outlet allowed particles to exit more easily and at higher velocities, reducing the likelihood of arching or stagnant zones near the outlet. Consequently, the particles in the vicinity of the outlet could move more freely, enlarging the region characterized by high particle velocities.

To facilitate a detailed comparison of particle velocity characteristics under different outlet diameters, the lateral distributions of particle velocity at two vertical positions were analyzed, as shown in Figure 8. At H = 3 m, the particle velocity distribution exhibited a clear M-shaped profile, and the velocity increased progressively with outlet diameter, as shown in Figure 8(a). Specifically, when D_o = 0.26 m, the peak velocity was approximately 0.12 m/s; when D_o = 0.52 m, the peak rose to about 0.30 m/s; and when D_o = 0.78 m, it further increased to nearly 0.90 m/s. Moreover, the velocity difference between the central region and the near-wall region became more pronounced as the outlet diameter increased. At H = 1.5 m, the radial velocity distributions within the two flow channels exhibited an inverted V-shaped profile, as shown in Figure 8(b). Compared with the particle

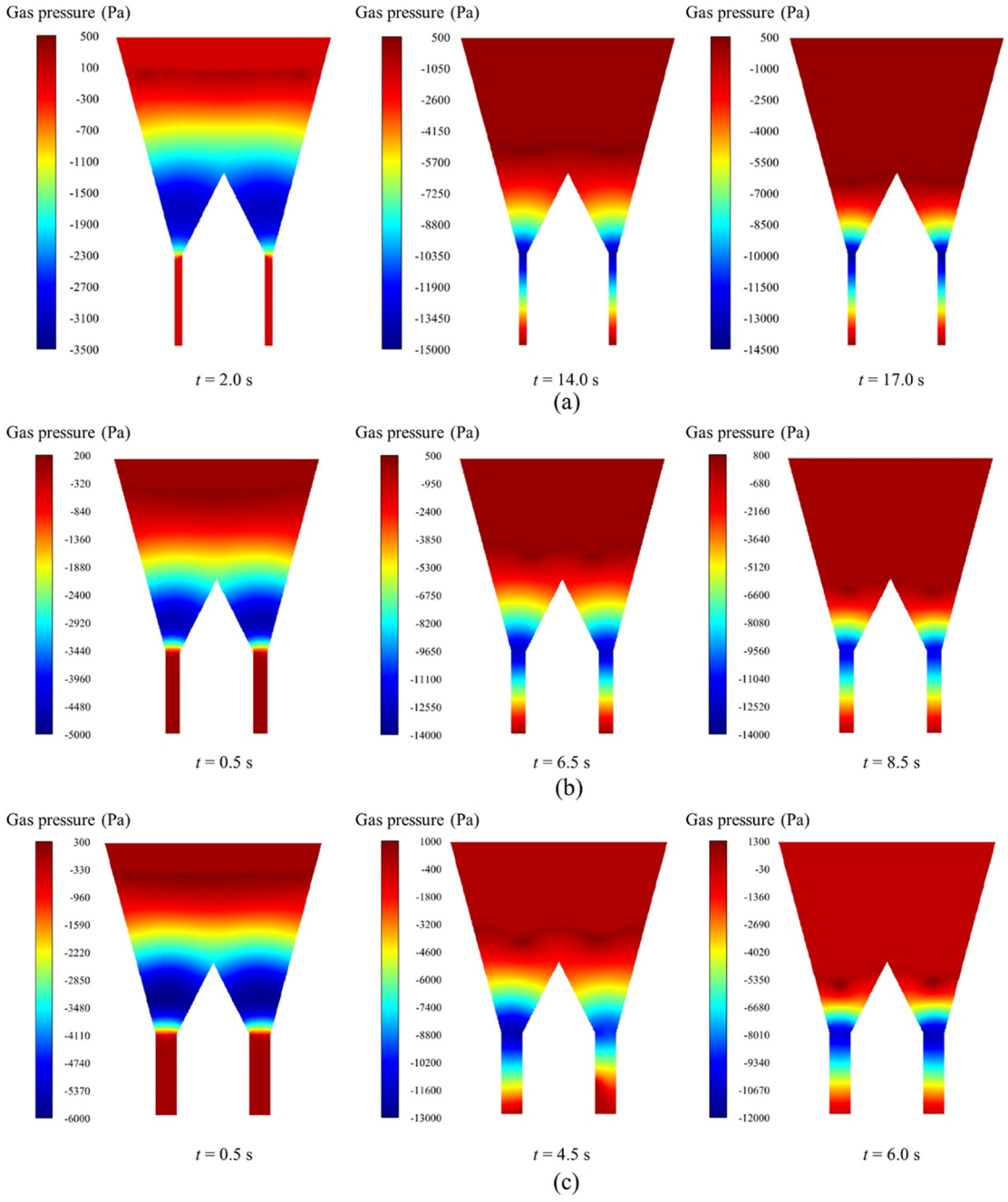


Figure 5. Contours of gas pressure in the hopper during discharge. (a) D_o = 0.26 m, (b) D_o = 0.52 m, (c) D_o = 0.78 m.

Source: Author's contribution.

velocity peaks at H = 3.0 m, the peak values at H = 1.5 m were higher under all outlet diameter conditions. Furthermore, the velocity difference between the central region and the near-wall region became more significant at this height, with the largest difference occurring when D_o = 0.78 m, reaching up to 1.45 m/s.

Figures 9 and 10 compare the gas and particle velocity distributions at different heights. At H = 3 m, for D_o = 0.26 m, the peak gas velocity was approximately 0.14 m/s, slightly higher than the corresponding particle velocity. In contrast, for D_o = 0.78 m, the peak gas velocity increased to about 0.90 m/s, nearly seven times that at D_o = 0.26 m. This

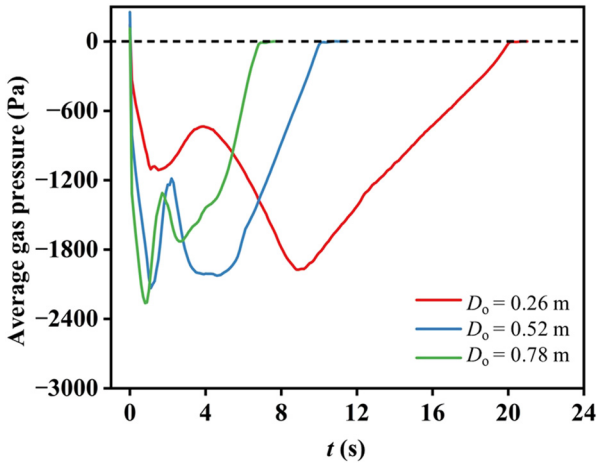


Figure 6. Average gas pressure in the silo system during discharge.

Source: Author's contribution.

increase indicates that a larger outlet significantly enhances gas flow acceleration and, consequently, particle entrainment, due to reduced outlet resistance and increased gas–solid drag interaction.

At a lower height (H = 1.5 m), both gas and particle velocities were greater than those at H = 3 m. Specifically, at D_o = 0.26 m, the peak velocity was approximately 0.21 m/s, while at = 0.78 m, it increased to about 1.50 m/s. Moreover, the velocity difference between gas and particles at this height became smaller. This reduction can be attributed to the denser particle packing in the lower region, which enhances interphase momentum exchange and leads to a more synchronized gas–solid motion. The results thus demonstrate that the outlet diameter affects not only the magnitude of flow velocities but also the coupling strength between the gas and particle phases during discharge.

3.4 Effect on the powder discharge characteristics

The outlet diameter has a significant effect on the discharge characteristics of the silo-to-vertical pipe powder conveying system. Figure 11(a) shows the variation of powder mass in the silo during discharge for different outlet diameters. It can be observed that the powder mass in the silo decreased more rapidly as the outlet diameter increased. When the outlet diameter was D_o = 0.26 m, the discharge time was approximately 20.0 s; for D_o = 0.52 m, the discharge time was about 10.0 s, representing a twofold reduction. When the outlet diameter was further increased to D_o = 0.78 m, the discharge time was reduced to approximately 7.5 s. This phenomenon can be attributed to several factors. First, a larger outlet increases the cross-sectional area through which particles can pass, thereby allowing a greater amount of material to discharge simultaneously. Second, the likelihood of arching or clogging decreases with outlet size, which promotes smoother and more continuous flow. Figure 11(b) presents the normalized discharge mass percentage of the silo powder. Similarly, it can be seen that increasing the outlet diameter significantly improved the discharge efficiency of the silo.

Figure 12 illustrates the variation of powder mass flow rates at each pipe outlet during discharge under different outlet diameters. It can be observed that, under the same operating conditions, the mass flow rate trends at the two vertical pipe outlets were generally consistent, both exhibiting an initial increase followed by a sharp decrease; however, the curves were not completely identical. This discrepancy was primarily attributed to the discharge competition effect in a dual-outlet silo, where the two outlets interacted during discharge, causing local flow states to shift and resulting in slight differences in the mass flow rates. Moreover, this competitive effect was less pronounced for the smaller outlet, indicating that outlet size played a key role in modulating the interaction between the two discharge channels. It is worth noting that the classical Beverloo equation provides an empirical estimate of discharge rate for nonaerated granular flows, whereas the present TFM explicitly considers gas–solid coupling and outlet pipe effects, which extend beyond the assumptions of the Beverloo formulation.

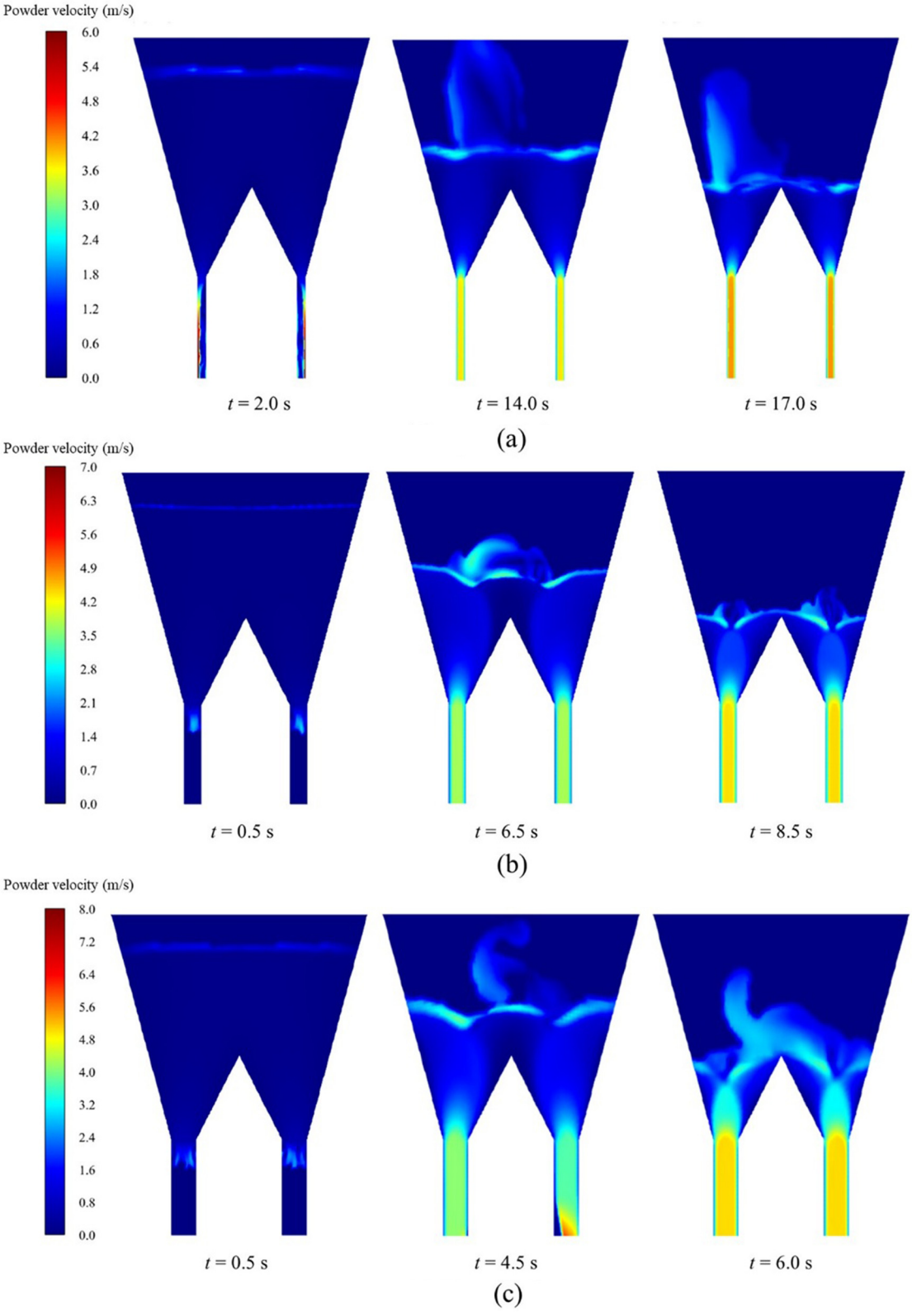


Figure 7. Contours of powder velocity in the silo system during discharge. (a) D_o = 0.26 m, (b) D_o = 0.52 m, (c) D_o = 0.78 m.

Source: Author's contribution.

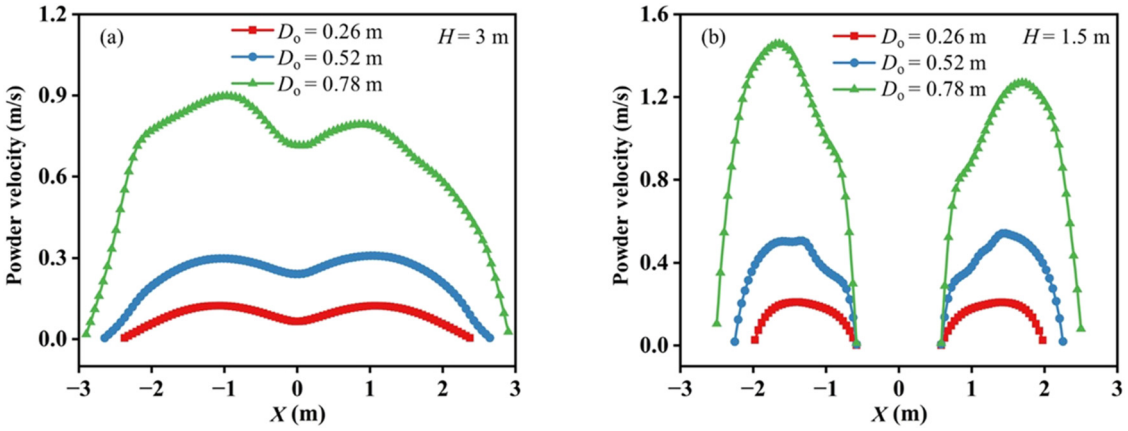


Figure 8. Powder velocity at discharge time t = 2.5 s. (a) H = 3.0 m, (b) H = 1.5 m.

Source: Author's contribution.

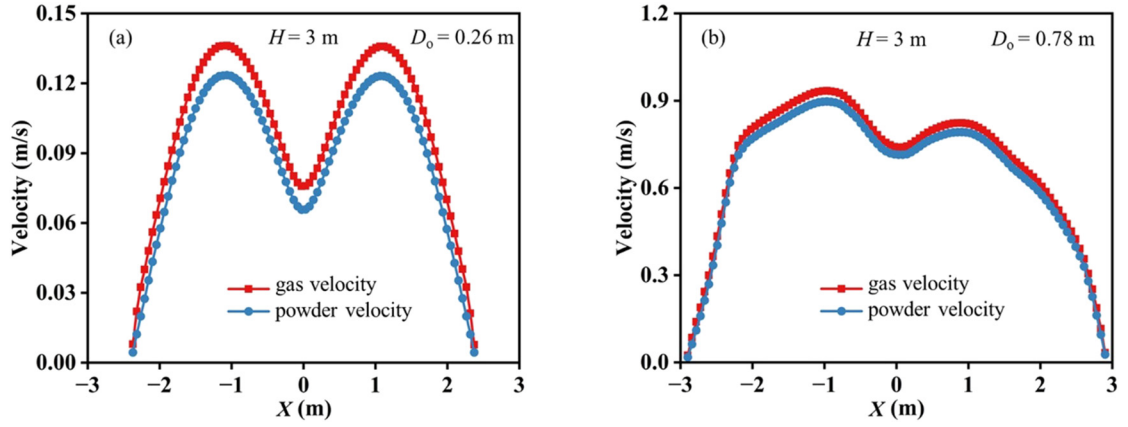


Figure 9. Gas and powder velocity at H = 3 m when t = 2.5 s. (a) D_o = 0.26 m, (b) D_o = 0.78 m.

Source: Author's contribution.

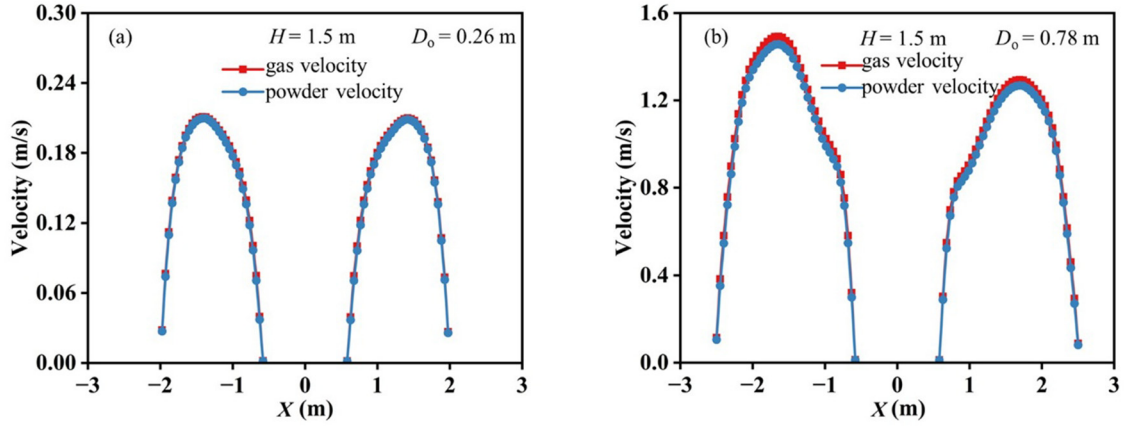


Figure 10. Gas and powder velocity at H = 1.5 m when t = 2.5 s. (a) D_o = 0.26 m, (b) D_o = 0.78 m.

Source: Author's contribution.

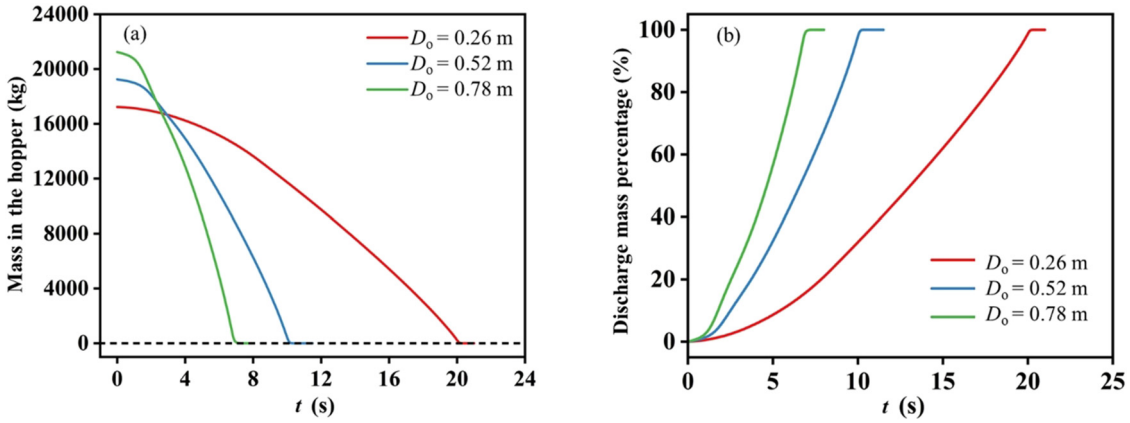


Figure 11. Discharge mass properties during the hopper emptying process. (a) Mass in the hopper, (b) discharge mass percentage.

Source: Author's contribution.

4. Conclusions

In the present study, a TFM was employed to numerically simulate the coupled flow process of powders and interstitial gas in a dual-outlet silo and its vertical pipes. By varying the outlet diameters, the effects on powder volume distribution, gas pressure evolution, particle velocity field, and overall discharge characteristics were analyzed. The main findings can be summarized as follows:

1. The outlet diameter exerts a significant influence on the evolution of powder volume fraction during silo discharge. A larger outlet not only accelerates the subsidence of the free surface and deepens the local depressions above the outlets but also shortens the time required for the free surface to reach the apex of the inverted V-shaped structure. The lateral distribution of powder volume fraction exhibits a characteristic W-shaped profile in the upper region and a V-shaped profile closer to the outlet, reflecting the combined effects of gravitational acceleration and structural configuration.
2. A negative gas pressure region consistently develops above the outlet at the onset of discharge and stabilizes at the hopper–pipe junction, owing to the imbalance between downward particle motion and insufficient air replenishment. At the initial stage of discharge, larger outlet diameters intensify the magnitude of the negative pressure peak because particles exit more rapidly. In addition, slight asymmetries in the pressure distribution between the two hoppers suggest

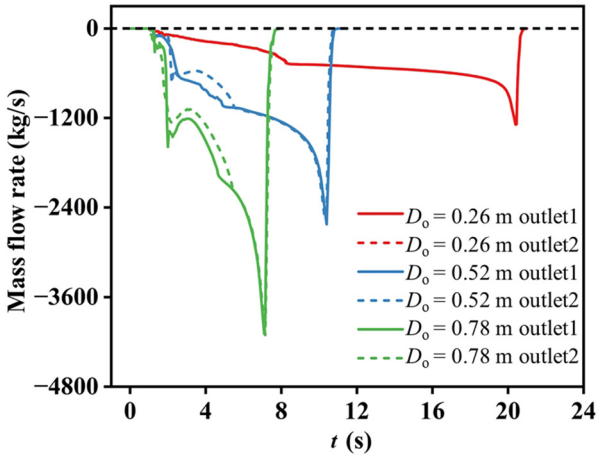


Figure 12. Mass flow rate properties during discharge.

Source: Author's contribution.

competitive discharge effects inherent to the dual-outlet configuration. Analysis of the temporal evolution of average gas pressure further reveals that, while fluctuations dominate the initial stage, the pressure exhibits a near-linear recovery in the later stages. A larger outlet not only accelerates the initial pressure reduction but also enhances the subsequent recovery rate by allowing faster air replenishment through interstitial spaces in the later stages of discharge. These findings demonstrate that outlet size critically governs both the spatial distribution and dynamic evolution of gas pressure in dual-outlet silo discharge.

3. When the outlet diameter increases from 0.26 to 0.78 m, the overall particle velocity increases significantly, with peak velocities at different heights enhanced by approximately seven times. At the initial stage of discharge, particle velocities in the silo region remain relatively uniform, whereas those in the pipe are less uniform. In the later stage, gas flow disturbances lift part of the particles upward. The enlargement of the outlet markedly promotes particle mobility, expanding the rapid-flow region near the outlet and reducing the likelihood of stagnant zones. The lateral velocity distributions exhibit characteristic M-shaped or inverted V-shaped profiles, indicating that the flow structure is jointly regulated by silo geometry and outlet size.
4. As the outlet diameters increase from 0.26 to 0.78 m, the powder discharge rate increases markedly, and the total emptying time reduces from ~22 to ~7 s, indicating a significant increase in discharge efficiency. During the discharge process, the mass flow rates of the two outlets show a generally consistent trend of first increasing and then decreasing, but with slight differences, reflecting a competitive discharge effect between the outlets. Within the range of outlet diameters investigated in this study, this competitive effect is less pronounced for the smaller outlet, indicating that outlet size plays a key role in modulating the interaction between the two discharge channels. Optimizing outlet diameter not only enhances discharge efficiency but also requires consideration of competitive flow effects in dual-outlet systems.

It should be noted that the present study has not included experimental validation of the proposed numerical model. Therefore, the results should be interpreted as model-based predictions. Nevertheless, the findings still provide meaningful insights into the underlying mechanisms and parameter sensitivities. Future work will focus on performing dedicated experiments to further verify and refine the model.

Funding information

Authors state no funding involved.

Author contributions

Xuanyi Liu: conceptualization, methodology, investigation, data curation, writing – original draft, supervision. Fei Wang: methodology, formal analysis, validation, writing – review & editing. Sijiu Qi: writing – review & editing.

Conflict of interest statement

Authors state no conflict of interest.

Data availability statement

Data will be made available on request.

References

[1] Agency, I.E., Status of power system transformation 2019; 2019. Retrieved September 21, 2025, from
[2] Schulze, D., Powders and bulk solids: Behavior, characterization, storage and flow, 2nd edn. Springer Nature Switzerland AG, Cham, Switzerland; 2021
[3] Jenike, A.W., Gravity flow of bulk solids; 1961. Retrieved September 20, 2025 from https://collections.lib.utah.edu/details? id=709033
[4] Jenike, A.W., Storage and flow of solids; 1964. Retrieved September 20, 2025, from https://digital.library.unt.edu/ark:/67531/metadc1067072
[5] Beverloo, W.A., Leniger, H.A., van de Velde, J., The flow of granular solids through orifices, Chem. Eng. Sci., 1961; 15(3): 260–269. doi: 10.1016/0009-2509(61)85030-6
[6] Wang, X., Shi, Y., Luo, B., Liang, C., Liu, D., Ma, J., et al., Flow profile and wall normal stress characteristics in pattern-transformable flow silos, Chem. Eng. Res. Des., 2022; 182: 381–394. doi: 10.1016/j.cherd.2022.04.019
[7] An, H., Wang, X., Fang, X., Liu, Z., Liang, C., Wall normal stress characteristics in an experimental coal silo, Powder Technol., 2021; 377: 657–665. doi: 10.1016/j.powtec.2020.09.016
[8] Wang, Y., Lu, Y., Ooi, J.Y. (2015). A numerical study of wall pressure and granular flow in a flat-bottomed silo, Powder Technol., 282: 43–54. doi: 10.1016/j.powtec.2015.01.078

[9] Chung, Y.C., Kuo, T.C., Hsiau, S.S., Effect of various inserts on flow behavior of Fe_2O_3 beads in a three-dimensional silo subjected to cyclic discharge- Part I: Exploration of transport properties, Powder Technol., 2022; 400: 117220. doi: 10.1016/j.powtec.2022.117220

[10] Krzyżanowski, J., Tejchman, J., Wójcik, M., Modelling of full-scale silo experiments with flow correcting inserts using material point method (MPM) based on hypoplasticity, Powder Technol., 2021; 392: 375–392. doi: 10.1016/j.powtec.2021.06.059

[11] Sun, D., Lu, H., Cao, J., Wu, Y., Guo, X., Gong, X., Flow mechanisms and solid flow rate prediction of powders discharged from hoppers with an insert, Powder Technol., 2020; 367: 277–284. doi: 10.1016/j.powtec.2020.03.053

[12] Liu, H., Han, Y., Jia, F., Xiao, Y., Chen, H., et al., An experimental investigation on jamming and critical orifice size in the discharge of a two-dimensional silo with curved hopper, Adv. Powder Technol., 2021; 32(1): 88–98. doi: 10.1016/j.apt.2020.11.020

[13] Guo, C., Ya, M., Xu, Y., Zheng, J., Comparison on discharge characteristics of conical and hyperbolic hoppers based on finite element method, Powder Technol., 2021; 394: 300–311. doi: 10.1016/j.powtec.2021.08.064

[14] Huang, X., Zheng, Q., Yu, A., Yan, W., Shape optimization of conical hoppers to increase mass discharging rate, Powder Technol., 2020; 361: 179–189. doi: 10.1016/j.powtec.2019.09.043

[15] Liu, H., Jia, F., Xiao, Y., Han, Y., Li, G., Li, A., et al., Numerical analysis of the effect of the contraction rate of the curved hopper on flow characteristics of the silo discharge, Powder Technol., 2019; 356: 858–870. doi: 10.1016/j.powtec.2019.09.033

[16] Wang, Y., Lu, Y., Ooi, J.Y., Finite element modelling of wall pressures in a cylindrical silo with conical hopper using an Arbitrary Lagrangian–Eulerian formulation, Powder Technol., 2014; 257: 181–190. doi: 10.1016/j.powtec.2014.02.051

[17] Wang, X., Liang, C., Guo, X., Chen, Y., Liu, D., Ma, J., et al., Experimental study on the dynamic characteristics of wall normal stresses during silo discharge, Powder Technol., 2020; 363: 509–518. doi: 10.1016/j.powtec.2020.01.023

[18] Wójcik, M., Tejchman, J., Enstad, G.G., Confined granular flow in silos with inserts – Full-scale experiments, Powder Technol., 2012; 222: 15–36. doi: 10.1016/j.powtec.2012.01.031

[19] Huang, X., Zheng, Q., Yu, A., Yan, W., Optimised curved hoppers with maximum mass discharge rate – an experimental study, Powder Technol., 2021; 377: 350–360. doi: 10.1016/j.powtec.2020.08.084

[20] Xu, L., Wu, X., Liang, J., Wang, S., Bao, S., Multi-level DEM study on silo discharge behaviors of non-spherical particles, Particuology, 2023; 82, 179–191. doi: 10.1016/j.partic.2023.02.001

[21] Pascot, A., Morel, J.-Y., Antonyuk, S., Jenny, M., Cheny, Y., Kiesgen De Richter, S., Discharge of vibrated granular silo: A grain scale approach, Powder Technol., 2022; 397: 116998. doi: 10.1016/j.powtec.2021.11.04

[22] Ketterhagen, W., Wassgren, C., A perspective on calibration and application of DEM models for simulation of industrial bulk powder processes, Powder Technol., 2022; 402: 117301. doi: 10.1016/j.powtec.2022.117301

[23] Wang, Y., Lu, Y., Ooi, J.Y., Numerical modelling of dynamic pressure and flow in hopper discharge using the Arbitrary Lagrangian–Eulerian formulation, Eng. Struct., 2013; 56: 1308–1320. doi: 10.1016/j.engstruct.2013.07.006

[24] Ma, H., Cai, W., Chen, J., Yao, Y., Jiang, Y., Numerical investigation on saturated boiling and heat transfer correlations in a vertical rectangular minichannel, Int. J. Therm. Sci., 2016; 102: 285–299. doi: 10.1016/j.ijthermalsci.2015.12.003

[25] Schneiderbauer, S., Pirker, S., A coarse-grained two-fluid model for gas-solid fluidized beds. J. Comput. Multiphase Flows, 2014; 6(1): 29–47. doi: 10.1260/1757-482x.6.1.29

[26] Hsiau, S.-S., Hsu, C.-C., Smid, J., The discharge of fine silica sands in a silo, Phys. Fluids, 2010; 22(4): 043306. doi: 10.1063/1.3394013

[27] Audard, F., Fede, P., Belut, E., Fontaine, J.-R., Neau, H., Simonin, O., Eulerian modelling of the powder discharge of a silo: Attempting to shed some light on the origin of jet expansion, Powder Technol., 2021; 379: 49–57. doi: 10.1016/j.powtec.2020.10.014

[28] Xu, C., Wang, F.-L., Wang, L.-P., Qi, X.-S., Shi, Q.-F., Li, L.-S., et al., Inter-orifice distance dependence of flow rate in a quasi-two-dimensional hopper with dual outlets, Powder Technol., 2018; 328: 7–12. doi: 10.1016/j.powtec.2018.01.019

[29] Dai, L., Yuan, Z., Fan, F., Gu, C., Experimental investigation on the gravity driven discharge of cohesive particles from a silo with two outlets, Particuology, 2024; 89: 11–21. doi: 10.1016/j.partic.2023.10.016

[30] Lee, M., Lee, S., Park, J., Prediction and validation of the profiles of the top and mixed loading surfaces during discharge from multiple-outlet silos, Adv. Powder Technol., 2023; 34(5): 104005. doi: 10.1016/j.apt.2023.104005

[31] Ishii, M., Hibiki, T., Thermo-fluid dynamics of two-phase flow, Springer New York, New York, USA; 2011
[32] Ding, J., Gidaspow, D., A bubbling fluidization model using kinetic theory of granular flow, AIChE J., 1990; 36(4): 523–538. doi: 10.1002/aic.690360404
[33] Johnson, P.C., Jackson, R., Frictional–collisional constitutive relations for granular materials, with application to plane shearing, J. Fluid Mech., 1987; 176: 67–93. doi: 10.1017/S0022112087000570
[34] Schneiderbauer, S., Aigner, A., Pirker, S., A comprehensive frictional-kinetic model for gas–particle flows: Analysis of fluidized and moving bed regimes, Chem. Eng. Sci., 2012; 80: 279–292. doi: 10.1016/j.ces.2012.06.041
[35] Srivastava, A., Sundaresan, S., Analysis of a frictional–kinetic model for gas–particle flow, Powder Technol., 2003; 129(1): 72–85. doi: 10.1016/S0032-5910(02)00132-8
[36] Gidaspow, D., Multiphase flow and fluidization: Continuum and kinetic theory descriptions, Academic Press, London, UK; 1994
[37] Wen, C.Y., Yu, Y.H., Mechanics of fluidization, In B.S. Lee (eds.), Fluid Particle Technology, Chemical engineering progress symposium series, American Institute of Chemical Engineers, New York, USA; 1966. pp. 100–111
[38] Ergun, S., Fluid flow through packed columns, Chem. Eng. Prog., 1952; 48(2): 89–94
[39] Vasquez, S.A., Ivanov, V.A., A phase coupled method for solving multiphase problems on unstructured meshes, In Revelling in reference: Proceedings of the ASME fluids engineering division summer meeting, American Society of Mechanical Engineers, Boston, Massachusetts, USA; 2000. pp. 734–748
[40] Wu, H.L., Peng, X.F., Ye, P., Eric Gong, Y., Simulation of refrigerant flow boiling in serpentine tubes, Int. J. Heat Mass Trans., 2007; 50(5): 1186–1195. doi: 10.1016/j.ijheatmasstransfer.2006.10.013
[41] Kunte, A., Doshi, P., Orpe, A.V., Spontaneous jamming and unjamming in a hopper with multiple exit orifices, Phys. Rev. E, 2014; 90(2): 020201. doi: 10.1103/PhysRevE.90.020201